Front. Phys., 2012, 7(5): 514–520
DOI 10.1007/s11467-012-0271-y

RESEARCH ARTICLE

Vibrational chaotic dynamics in triatomic molecules: A comparative study

Liang-Jun Zhai (翟良君), **Yu-Jun Zheng** (郑雨军)†, **Shi-Liang Ding** (丁世良)

School of Physics, Shandong University, Jinan 250100, China

E-mail: †*yzheng@sdu.edu.cn*

Received May 2, 2012; accepted June 10, 2012

Within Lie algebraic model, the vibrational chaotic dynamics in triatomic molecules are studied. The molecules of H_2S, NO_2, and O_3 are sampled to explore the dynamical differences between the local and normal mode molecules. The comprehensive effects of the local and normal mode vibrations, resonances and chaos on the dynamical entanglement are studied. The results demonstrate that the resonances as well as chaos can promote the evolution of dynamical entanglement.

Keywords vibrational chaotic dynamics, triatomic atomic, $U(4)$ algebraic model

PACS numbers 05.45.Ac, 05.45.Mt, 33.20.Tp

1 Introduction

The molecules can be defined as the local and normal mode molecules because of the differences of their vibrational spectroscopy [1, 2]. The striking feature of local mode molecules is that the splitting between the lowest members in each of the overtone manifolds is rapidly decreasing with the increase of total quantum numbers [3], while the corresponding splitting can hardly decrease for the normal mode molecules [4]. On the other hand, the dynamical studies have shown that their dynamical behaviors are also significantly different [2, 5, 6]. One usual method to extract dynamical information from the quantum energy levels is via the classical–quantum approach [7–9], which can provide a vivid picture of molecular dance. There are many pathways to investigate the classical–quantum correspondence, such as the dynamics in the quantum phase space [10], etc. The analysis of the phase structure is an effective method to investigate the molecular dynamics [8]. By the method of Poincaré section, the phase structures of local mode molecules have been discussed based on the local mode description. However, for the normal mode molecules, there are still many open questions, such as the normal-to-local mode transition at higher energies [4, 11] and the irregular tori on the Poincaré section [12]. Recent studies have also highlighted the importance of quantum dynamical entanglement as an indicator of the underlying classical dynamics [13–15]. The researches have shown that the degree of entanglement is the largest when the initial state lies at the edge of regular islands or in the chaotic sea [16, 17].

The Lie algebraic model of molecules has been proven to be an effective model in the description of vibrations in polyatomic molecules [18–20]. The Lie algebraic model has a simple form in description, and the anharmonicities of each mode and resonances between different modes can be introduced automatically by the matrix elements of operators [21]. Because of those advantages, the algebraic method has extensive applications from small molecules to molecular chains [22–28], and other questions on molecular physics [5, 29, 30].

In this paper, the vibrational chaotic dynamics of the small molecular system are investigated based on the Lie algebraic model. The comparative study about the dynamical differences of the local and normal mode molecules are considered. And the comprehensive effects of the global effects of classical dynamics on the entanglement are discussed by studying the linear entropies of coherent states.

The organization of the paper is as follows. In Section 2, the $U(4)$ algebraic Hamiltonian for symmetrical bent triatomic molecules is reviewed, and the classical limit of Hamiltonian is also given based on $U(4)$ algebraic Hamiltonian in this section. In Section 3, the phase structures of the three triatomic molecules are depicted by the Poincaré sections, and the effects of global dynamics on the generation of entanglement are also discussed.

A brief summary is presented in Section 4.

2 Theoretical framework

For a triatomic molecule, a $U(4)$ algebra is introduced to describe the three mechanical degrees of freedom of each bond. The dynamical group is $U_1(4) \otimes U_2(4)$ (we denote the left bond of triatomic molecules as bond 1, and the right bond as bond 2), and the dynamical symmetric chains are written as [20]

$$\begin{aligned} &U_1(4) \otimes U_2(4) \supset U_{12}(4) \supset O_{12}(4) \\ &U_1(4) \otimes U_2(4) \supset O_1(4) \otimes O_2(4) \supset O_{12}(4) \end{aligned} \tag{1}$$

The quantum Hamiltonian, based on the $U(4)$ algebraic model, is expressed as [20]

$$H = A_1 C_1 + A_2 C_2 + A_{12} C_{12}^{(1)} + A'_{12} C_{12}^{(2)} + \lambda M_{12} \tag{2}$$

where A_1, A_2, A_{12}, A'_{12}, and λ are the expansion coefficients which can be determined by fitting the spectroscopic data. C_1 and C_2 are Casimir operators of groups $O_1(4)$ and $O_2(4)$, respectively; $C_{12}^{(1)}$ and $C_{12}^{(2)}$ are two Casimir operators of $O_{12}(4)$; and M_{12} is the Majorana operator denoting the coupling between two bonds. The explicit form of the matrix elements can be found in Ref. [24].

2.1 Classical limit of algebraic Hamilton and chaotic dynamics

To describe the classical chaotic dynamics of intramolecular vibrations, we need to find the classical limits of algebraic Hamiltonian of Eq. (2). Following the approach of *intensive boson operators* introduced by Gilmore [31], the classical limits of algebraic Hamiltonian (2) are obtained via

$$H_{cl} = H(\boldsymbol{z}, \boldsymbol{z}^\dagger) \tag{3}$$

where $\boldsymbol{z}$ is a complex quantity, and $\boldsymbol{z}^\dagger$ is its corresponding complex conjugate. By considering the canonical coordinates through the canonical transformation, the classical limit of algebraic Hamilton Eq. (3) can be written as the usual form in molecular coordinates as follows [32]:

$$H_{cl} = V + T \tag{4}$$

The potential energy V reads as

$$\begin{aligned} V(y_1, y_2) = {} & a_0 + D_1 y_1^2 + D_2 y_2^2 \\ & + a_{12}^0 y_1 y_2 + a_{12}^1 \left[(1-y_1^2)(1-y_2^2)\right]^{\frac{1}{2}} \end{aligned} \tag{5}$$

where $y_i = 1 - \mathrm{e}^{-\beta_i(r_i - r_{ie})}$ $(i = 1, 2)$ is the Morse variables; r_1 and r_2 are bond lengths, and β_i is the Morse steepness parameters; r_{ie} is equilibrium bond length. The other parameters are deduced from the coefficients in the quantum Hamiltonian Eq. (2), namely, $a_0 = (A_1 + A_{12})N_1^2 + (A_2 + A_{12})N_2^2 + \frac{1}{2}\lambda N_1 N_2$; $a_{12}^0 = -\frac{1}{2}\lambda N_1 N_2$ and $a_{12}^1 = (2A_{12} - \frac{1}{2}\lambda)N_1 N_2$; $D_i = -(A_i + A_{12})N_i^2, i = 1, 2$ is the single bond's dissociation energy. The general properties of the potential energy of Eq. (5) are studied in Refs. [24–26], and they have been successfully applied in determining the potential energy surfaces of both local and normal mode triatomic molecules [24–28].

In the case of frozen bond angle, the kinetic term of triatomic molecules in the intramolecular coordinates is

$$\begin{aligned} T(p_1, p_2) = {} & \frac{1}{2}\left[(\mu_1 + \mu_3)p_1^2 + (\mu_2 + \mu_3)p_2^2\right] \\ & + \mu_3 \cos(\phi_0) p_1 p_2 \end{aligned} \tag{6}$$

where p_1 and p_2 are the momentum of two bonds, $\mu_1 = 1/m_1$, $\mu_2 = 1/m_2$, m_1 and m_2 are the masses of the atoms at the two ends of bonds; $\mu_3 = 1/M$, and M is the mass of central atom and ϕ_0 is the equilibrium bond angle. In the present study, the triatomic molecules H_2S, NO_2, and O_3 are sampled, and parameters taken from Refs. [24, 27, 28] of the three molecules in Eqs. (2) and (5) are listed in Table 1. These parameters are representing the natures of vibrational lines and potential energy surfaces of the three molecules [24, 27, 28].

Table 1 The parameters of the triatomic H_2S, NO_2, and O_3. [1)]

Molecule	N_i	β_i	A_i	A_{12}	λ	r_{ie}	ϕ_0
H_2S	40	1.93	−13.57	−2.14	0.458	1.34	1.6057
NO_2	115	3.4507	−1.9052	0.0055	−0.6369	1.1872	2.3439
O_3	70	2.679	−11.6522	2.9914	−3.0782	1.2075	2.0385

Note: [1)] $i = 1$ and 2 are the two bonds in molecules. A_i, A_{12}, λ are in cm^{-1}; β_i is in $\mathrm{Å}^{-1}$; r_{ie} is in Å; ϕ_0 is in rad.

2.2 Local mode parameter of a molecule

The local mode parameter $\xi = -\chi/\lambda_{rr'}$ is proposed to identify the local and normal mode molecules [1], where χ is the bond's anharmonicity parameter and $\lambda_{rr'}$ is the coupling coefficient between the two bonds. For the molecules in normal mode limit $|\xi| \ll 1$, while the opposite happens in the case of local mode limit molecules. The anharmonicity parameter in the $U(4)$ algebraic model is expressed as

$$\chi_i = -4(A_i + A_{12}) \tag{7}$$

And the coupling parameter between the two bonds is expressed as

$$\begin{aligned} \lambda_{rr'} &= \frac{1}{2}\omega_i \left(\frac{g_{rr'}^{(e)}}{g_{rr}} + \frac{f_{rr'}^{(e)}}{f_{rr}}\right) \\ &= \frac{1}{2}\omega_i \left[\frac{\left(\dfrac{\partial^2 T}{\partial p_1 \partial p_2}\right)_e}{\left(\dfrac{\partial^2 T}{\partial p_i^2}\right)_e} + \frac{\left(\dfrac{\partial^2 V}{\partial r_1 \partial r_2}\right)_e}{\left(\dfrac{\partial^2 V}{\partial r_i^2}\right)_e}\right] \end{aligned} \tag{8}$$

where $\omega_i = -4(A_i + A_{12})N_i$ is the harmonic wavenumber of a single bond. The superscript (or subscript) e denotes

that the molecule located at equilibrium position. Then, the local mode parameter, under the algebraic model, is written as

$$\xi^{-1} = \frac{N_i \mu_3 \cos\phi_0}{\mu_1 + \mu_3} + \frac{\lambda N_i^3 \beta_i^2}{4(A_i + A_{12}) + 4A_{12}N_i^2\beta_i^2 - \lambda N_i^2 \beta_i^2} \quad (9)$$

χ_i, $\lambda_{rr'}$, and ξ for three molecules are tabulated in Table 2.

Table 2 χ_i, $\lambda_{rr'}$, and ξ for H_2S, NO_2, and O_3. [1)]

Molecule	χ_i	$\lambda_{rr'}$	ξ
H_2S	−62.84	−9.3396	−6.7283
NO_2	−7.5988	−122.6529	−0.0620
O_3	34.6432	−82.9153	0.4178

Note: [1)] $i = 1$ and 2 are the two bonds in molecules.

3 Chaotic dynamics of molecular vibrations in phase structures

The bond coordinates r_i and momenta p_i satisfy Hamiltonian's canonical equations. Through the numerical integration, the intramolecular classical dynamics are obtained. By employing the method of Poincaré section, the phase structures of each energy level are presented. The Poincaré section is a useful method in discussing the chaos in the low dimensional systems. For a Hamiltonian with two degrees of freedom, because the energy is conserved, the trajectories can spread in three dimensional phase space. We then define the Poincaré section as the section of $r_2 = r_{2e}$ in the phase space so that every time a trajectory pierces this section with $p_2 > 0$ the corresponding point (r_1, p_1) is plotted. Generally speaking, there are periodical points, quasi-periodical tori, islands chains and irregular points on the Poincaré section. For the intramolecular vibrations, they are corresponding to the periodical vibration, quasi-periodical vibration, nonlinear resonances and chaotic vibrations, respectively.

3.1 Basic structures of local and normal mode molecules in phase space

With the aim to present the basic structures of the Poincaré sections of the local and normal mode molecules, we sample two typical sections of H_2S and NO_2 molecules to make the discussion which are plotted in Fig. 1.

Panel (a) of Fig. 1 presents that the Poincaré section of H_2S with total vibrational energy (TVE) is at 2164.41 cm^{-1}. This section shows a typical structure of the local mode molecule, which can be simply divided into three regions [33]: two local mode regions (yolk and shell parts of the section), and the antisymmetrical normal mode region lain between them. From the viewpoint of IVR, in the local mode regime, once the bond is excited, the energy remains localized in that bond with fairly small fluctuation [34]. But the energy exchanges freely for the normal mode vibration. However, even in the local mode regions, our calculation shows that the two bonds are vibrating with similar frequencies. This means that the energy discrepancy is not high enough to result in a discrepancy of frequency. This type of vibration is named as the quasi-local mode vibrations by Kryvohuz and Cao recently [35].

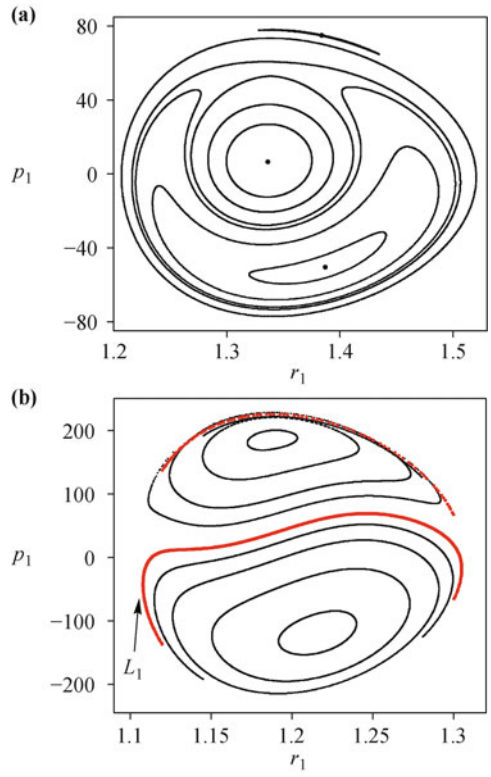

Fig. 1 Typical Poincaré sections of the local and normal mode molecules. Panel **(a)** is section of H_2S computed at TVE=2164.41 cm^{-1}, and panel **(b)** is the section of NO_2 with TVE=2627.34 cm^{-1}. The red line in panel (b) denotes the fractured torus of the normal mode molecules.

For normal mode molecules, the Poincaré sections are different from the local mode molecules. The Poincaré section of NO_2 with TVE= 2627.34 cm^{-1} is shown in Fig. 1(b). The section is clearly divided into the symmetric (the upper semi-sphere) and antisymmetric (the under semi-sphere) regions of normal vibrational modes. It should be noted that some unclosed tori appear at the borders of the two normal mode regions, and tori can cross with each other at the upper border of the symmetrical normal mode region. Actually, two of these isolated segments belong to one trajectory. Namely, the half of red torus L_1, as shown in Fig. 1(b), locates at the border of the antisymmetrical normal mode region, and the other half appears at the border of symmetrical normal mode region. In the following discussion, we name this type of tori as the "fractured tori".

In the local mode description, each bond of the triatomic molecule is seen as an isolated Morse oscillator, and the usual description of bond's vibrational energy is defined as follows

$$H_i(y_i, p_i) = a_i y_i^2 + \frac{1}{2}(\mu_i + \mu_3)p_i^2, \quad i = 1, 2 \tag{10}$$

Due to the coupling in the triatomic system, bonds' energies depend on each other. We name here the energy defined via Eq. (10) as the "bond's energy-like" in the following discussion.

From the observation of the bonds' energy-like, the fractured tori often have a distinctive feature that one bond is firstly excited. Such fractured tori phenomenon is a dynamical distinguishing characteristic of the initial local-mode character and normal-mode character vibration in normal mode molecules. And, the rate of energy transfer between bonds of the initial normal-mode character states is more rapid than that of the initial local mode states.

3.2 Chaotic dynamics of local mode molecule: Case study of H_2S

The resonance islands appear on the section of H_2S for the first time when TVE is around 15 000 cm^{-1}, and the total quantum number N of the stretching vibration is around 6. Panel (a) of Fig. 2 is the section of TVE = 18 276.7 cm^{-1}. Two observable resonance islands chains emerge on the Poincaré section: the (3 : 2) resonance chain (labeled as red tori) in the yolk part and the (2 : 3) (labeled as the blue tori) resonance chain located in the shell, where the ratio (3 : 2) [or (2 : 3)] is used to denote the relationship of the bonds' vibrational frequencies.

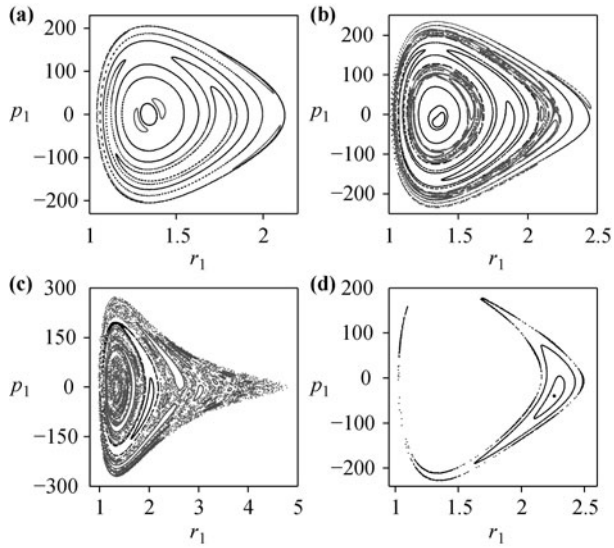

Fig. 2 Poincaré sections of H_2S molecule. The TVE of H_2S are: 18 276.7 cm^{-1} for panel **(a)**, 23 571 cm^{-1} for panel **(b)**, 31 984 cm^{-1} for panel **(c)** and 41 235 cm^{-1} for panel **(d)**, respectively. The blue lines in the panels denote the nonlinear resonance island chains, while the red irregular points are the chaotic trajectories.

The appearance of these resonance islands means that the vibrational frequency discrepancy between bonds come forth, which is caused by the energy discrepancy. With the growth of TVE, more and more resonance islands appear on the Poincaré section, and the chaotic trajectories are originated in the overlapping regions of the resonances [36]. In panel (b) of Fig. 2, the section of TVE= 23 571.0 cm^{-1} is plotted. The chaotic trajectories (labeled as red trajectories) appear around some major resonance islands. In such energy range, the local mode vibration takes the main region on the Poincaré section. The long time averaged energy discrepancy between two bonds is also increasing with the growth of TVE.

We define here the effective bond's depth D_{eff} of the single bond, which is written as

$$\begin{aligned} D_{\text{eff}} &= V(r_1 \to \infty, r_2 = r_{2e}) - V(r_1 = r_{1e}, r_2 = r_{2e}) \\ &= -(A_1 + A_{12})N_1^2 + \left(\frac{1}{2}\lambda - 2A_{12}\right)N_1 N_2 \end{aligned} \tag{11}$$

When TVE is around D_{eff}, the vibration is chaotic. For H_2S, D_{eff} = 32 350.4 cm^{-1}. Panel (c) of Fig. 2 presents the Poincaré section with H_2S for TVE = 31 984 cm^{-1}. Although the surface is dominated by the chaotic trajectories, the resonance islands have still arisen. When TVE is far above D_{eff}, due to the local mode nature, the tori originated in the local mode regions can cause that the "bond's energy-like" is higher than the D_{eff}. Its consequence is that most of the chaotic and local mode tori tend to disappear on the Poincaré section. The Poincaré section of H_2S for TVE = 41 235 cm^{-1} is displayed in panel (d) of Fig. 2, where only the antisymmetrical normal mode region exists. Such section means that the vibration of H_2S draws back to regular in the high excited states.

3.3 Chaotic dynamics of the normal mode molecules: Case study of NO_2

The Poincaré sections of NO_2 with higher energy are still composed of the normal mode regions. Panel (a) of Fig. 3 is the section of TVE=7228.5 cm^{-1}. The resonance islands turn up at the unstable symmetrical normal region, and they are fractured as well. One chain of fractured islands is sampled as the blue torus shown in panel (a). When the Poincaré section is dominated by the chaotic trajectories, the fracture phenomenon can be concealed by the irregular points of the chaotic tori. In panel (b) of Fig. 3, the Poincaré section of TVE = 10 152.3 cm^{-1} is plotted. But we can find a region (using red points) with much denser points which is the tori cross region, and the bonds' energy-like is higher than TVE in such region.

Panels (c) and (d) of Fig. 3 give the transformation of the chaotic trajectories when TVE is near D_{eff}. Different from H_2S, the chaotic trajectories of NO_2 can dif-

fuse all over the symmetric normal mode region, and the resonance islands all fade away by chaotic trajectories. However, the antisymmetrical normal mode region always exists on the section. When TVE transcends the D_{eff}, there are only anti-symmetrical normal mode region left on the section. Panel (d) of Fig. 3 shows this case.

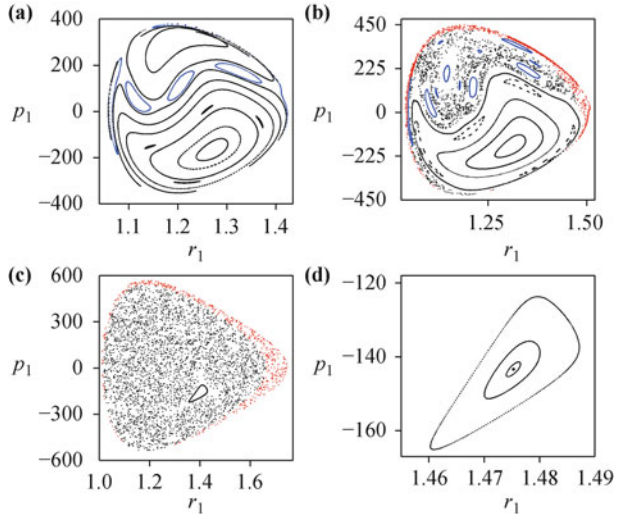

Fig. 3 Poincaré sections of NO_2 molecule. The TVE of NO_2 are: 7228.6 cm^{-1} for panel **(a)**, 10 152.3 cm^{-1} for panel **(b)**, 16 311.6 cm^{-1} for panel **(c)** and 22 000 cm^{-1} for panel **(d)**, respectively. Here, the blue lines in panels (a) and (b) are denoting the resonance islands, while the crossing regions of the chaotic trajectories are labeled as the red points in panels (b) and (c).

3.4 Chaotic dynamics of intermediate of local and normal mode limits: Case study of O_3

The Poincaré sections of O_3 are displayed in Fig. 4. With low TVE, as shown in panel (a) of Fig. 4, the section is composed of the symmetric and antisymmetric normal mode regions. The fractured tori also arise at the border of the normal mode regions which are the typical tori of the normal mode molecules. However, as TVE grows higher, the quasi-local mode tori begin to appear on the section. As shown in panel (b) of Fig. 4, the section of TVE = 6173.8 cm^{-1} has a structure of local mode molecules. Meanwhile, the resonance islands and chaotic tori begin to appear around such TVE, but there is no significant frequencies difference between the vibrations of two bonds. The appearance of the fractured tori (the red tori) on the shell part means that the vibration has dual characters of local and normal mode molecules.

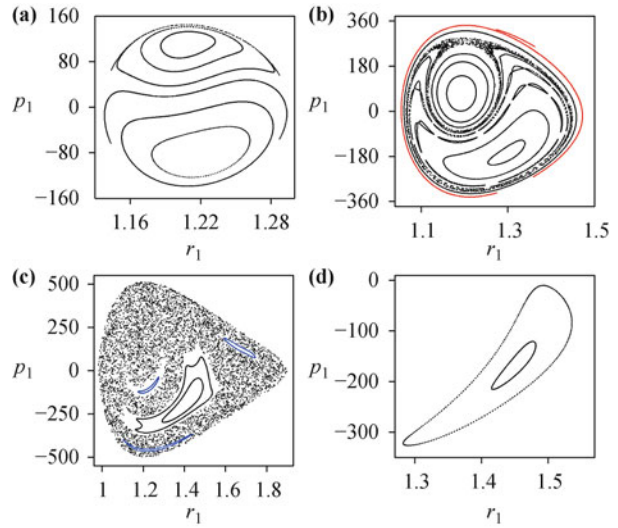

Fig. 4 Poincaré sections of O_3 molecule. The TVE of O_3 are: 1044.3 cm^{-1} for panel **(a)**, 6173.8 cm^{-1} for panel **(b)**, 13 122 cm^{-1} for panel **(c)** and 15 000 cm^{-1} for panel **(d)**, respectively. The red line in panel (b) denotes the fractured tori of quasi-local mode vibration. The blue lines in panel (c) are denoting the resonance islands.

Panel (c) of Fig. 4 gives the sections of O_3 with TVE = 13 122 cm^{-1}, where the widespread chaos appear on the section. The entire surface of section is similar to the highly excited states of NO_2, but some resonance have islands still survived, which are different with NO_2. When TVE = 15 000 cm^{-1}, which is above the D_{eff}, the chaotic tori disappear.

3.5 Global effects of classical dynamics on dynamical entanglements

Recently, several researchers have also proposed to apply the quantum–classical correspondence to study the dynamical entanglement, which allows us to compute and interpret the properties of a quantum system in terms of the properties of its classical counterpart. Initially, the early researches on some nonlinear models, which include the coupled kicked tops [15], the Dicke model [37], and Jaynes–Cumming model [38], have supported that the classical chaos can induce a stronger entanglement. However, exceptions have been found in recent studies [39, 40]. In their studies, it is found that the entanglement is insensitive toward the choice of regular or chaotic initial condition but is highly determined the global dynamics [39].

For the molecular systems, extensive investigations have found that the classical nonlinear resonances as well as the classical chaos have great impact on the intramolecular dynamics [41]. However, there are seldom works done to find the relationships between the classical chaos and the dynamical entanglement [32]. Physically, entanglement between bonds can be interpreted the interdependence between bonds. Therefore, it is important to explore the relations between the classical dynamics and the dynamical entanglement. In our previous study, we have found that the classical local mode vibration corresponds to the long beats in the generation of dynamical entanglement, and the maximum value of entanglement always appears in the transition regions from the local-mode character states to the normal-mode character states.

In the present study, alternatively, the global effects

of the nonlinear resonances and chaos are explored by employing the following coherent states:

$$|\psi(0)\rangle = \mathrm{e}^{-\frac{|\alpha|^2}{2}} \sum_{n}^{N} \frac{\alpha^n}{\sqrt{n!}} |n, N-n\rangle \tag{12}$$

where α is a parameter denoting the amplitude of the coherent states. Here, we set α to be the maximum real number satisfying $\langle\psi(0)|\psi(0)\rangle \approx 1$. And N varies from 1 to 18. In the TVE range confined by N, this state could be the bridge connecting the quantum and classical dynamics. Here, we use the linear entropy and its long time-average to characterize the degree of entanglement between the stretching bonds.

It is seen that the degree of entanglement of H_2S is much smaller than NO_2 and O_3. When N is larger than 6, the local mode tori begin to appear on the section of O_3. Correspondingly, the degree of entanglement of O_3 begins to decrease as well. The results show that the local mode vibration can decrease the entanglement. On the other hand, for the local mode molecule H_2S, there is a significantly increase of long time-averaged linear entropy, while the resonance islands as well as chaos begin to appear on the Poincaré sections. Such correspondence demonstrates that resonance island as well as chaos can promote the generation of entanglement.

4 Conclusion

In this paper, the H_2S, NO_2, and O_3 are selected as examples to give a comparative discussion about the chaos of local and normal mode triatomic molecules. For the normal mode molecule NO_2, the fractured tori are found, and tori can cross with each other in specific areas. By the analysis of their underlying dynamics, it is shown that the bond's energy-like can exceed TVE. The strange behavior remands us that the bonds' energy should be specificly concerned when we apply the local mode description to the normal mode molecules. By the study of dynamical entanglement the degree of entanglement is in a low level when the local mode vibration appears. In addition, the chaos and resonance are found to have greatly promoted on the evolution of dynamical entanglement.

The small molecule is a system with potential applications in quantum computations. Since the intramolecular vibrational dynamic is one of the decoherence sources of quantum computation and quantum information, researches on the intramolecular vibrational dynamic are necessary for the molecular system. The $U(4)$ algebraic model is suitable to treat the bending vibration as well as the rotation, therefore as an extension of this work the decoherence dynamics will be studied in the framework of $U(4)$ algebraic model.

Acknowledgements This work was supported by the National Natural Science Foundation of China (Grant Nos. 91021009 and 10874102).

References

1. L. Halonen, Adv. Chem. Phys., 1998, 104: 41
2. T. Sako, K. Yamanouchi, and F. Iachello, J. Chem. Phys., 2000, 113(17): 7292
3. P. Jensen, S. Tashkun, and V. Tyuterev, J. Mol. Spectrosc., 1994, 168(2): 271
4. G. Ma, R. Chen, and H. Guo, J. Chem. Phys., 1999, 110(17): 8408
5. Y. Liu, Y. Zheng, W. Ren, and S. Ding, Phys. Rev. A, 2008, 78(3): 032523
6. F. Mauguiere, M. Rey, V. Tyuterev, J. Suarez, and S. C. Farantos, J. Phys. Chem. A, 2010, 114(36): 9836
7. K. K. Lehmann, G. J. Scherer, and W. Klemperer, J. Chem. Phys., 1982, 77(6): 2853
8. Z. Lu and M. E. Kellman, J. Chem. Phys., 1997, 107(1): 1
9. F. Iachello and F. Pérez-bernal, Mol. Phys., 2008, 106(2–4): 223
10. S. Keshavamurthy and G. S. Ezra, Chem. Phys. Lett., 1996, 259(1–2): 81
11. X. Hou, J. Chen, and Z. Ma, Phys. Rev. A, 2006, 74(6): 062513
12. L. Zhai, Y. Zheng, and S.L. Ding, Chin. Phys. Lett., 2012, 29(6): 063301
13. S. Chaudhury, A. Smith, B. E. Anderson, S. Ghose, and P. S. Jessen, Nature, 2009, 461(7265): 768
14. S. Ghose, R. Stock, P. Jessen, R. Lal, and A. Silberfarb, Phys. Rev. A, 2008, 78(4): 042318
15. X. Wang, S. Ghose, B. C. Sanders, and B. Hu, Phys. Rev. E, 2004, 70: 016217
16. H. Fujisaki, T. Miyadera, and A. Tanaka, Phys. Rev. E, 2003, 67: 066201
17. S. Zhang and Q. Jie, Phys. Rev. A, 2008, 77(1): 012312
18. F. Iachello and R. D. Levine, J. Chem. Phys., 1982, 77(6): 3046
19. O. S. van Roosmalen, F. Iachello, R. D. Levine, and A. E. L. Dieperink, J. Chem. Phys., 1983, 79(6): 2515
20. F. Iachello, and R. D. Levine, Algebraic theory of molecules, New York: Oxford University press, 1995
21. F. Iachello and S. Oss, Eur. Phys. J. D, 2002, 19: 307
22. F. Iachello and P. Truini, Ann. Phys., 1996, 276(1): 120
23. Y. Zheng and S. Ding, Phys. Lett. A, 1999, 256(2–3): 197
24. S. Ding and Y. Zheng, J. Chem. Phys., 1999, 111(10): 4466
25. Y. Zheng and S. Ding, J. Mol. Spectrosc., 2000, 201(1): 109
26. Y. Zheng and S. Ding, Phys. Rev. A, 2001, 64(3): 032720
27. Y. Zheng and S. Ding, Chem. Phys., 2000, 255(2–3): 217
28. Y. Zheng and S. Ding, Int. J. Quantum Chem., 2008, 108(6): 1059
29. Y. Zheng, Multiphoton Selective excitation and analytical control of small molecules in intense laser fields: an Algegraic model, in: Laser Pulse phenomena and Applications, edited by F. J. Duarte, INTECH, Rijeka, 2010

30. H. Feng, P. Li, and Y. Zheng, Mol. Phys., 2011, 109(22): 2633
31. R. Gilmore, Catastrophe Theory for Scientists and Engineers, New York: Dover Publications, 1981
32. L. Zhai, Y. Zheng, and S.L. Ding, Chin. Phys. B, 2012, 21(7): 070503
33. C. Jaffé and P. Brumer, J. Chem. Phys., 1980, 73: 5646
34. W. P. Sibert, Reinhardt, and J. T. Hynes, J. Chem. Phys., 1982, 77(7): 3583
35. M. Kryvohuz and J. Cao, J. Phys. Chem. B, 2010, 114(19): 6549
36. B. V. Chirikov, Phys. Rep., 1979, 52(5): 263
37. X. Hou and B. Hu, Phys. Rev. A, 2004, 69(4): 042110
38. R. M. Angelo, K. Furuya, M. C. Nemes, and G. Q. Pellegrino, Phys. Rev. A, 2001, 64(4): 043801
39. N. N. Chung and L. Y. Chew, Phys. Rev. E, 2009, 80: 016204
40. M. Lombardi and A. Matzkin, Phys. Rev. E, 2011, 83: 016207
41. S. Keshavamurthy, Int. Rev. Phys. Chem., 2007, 26(4): 521